Sensors and Actuators B 207 (2015) 74–82

Contents lists available at ScienceDirect

Sensors and Actuators B: Chemical

journal homepage: www.elsevier.com/locate/snb

Microwave-assisted synthesis of high-quality CdTe/CdS@ZnS–SiO_2 near-infrared-emitting quantum dots and their applications in Hg^{2+} sensing and imaging

Jing Wang[a,b], Na Li[a], Feng Shao[a], Heyou Han[a,*]

[a] State Key Laboratory of Agricultural Microbiology, College of Science, Huazhong Agricultural University, Wuhan, 430070, PR China
[b] College of Chemical Engineering, Zhejiang University of Technology, Hangzhou, 310014, PR China

ARTICLE INFO

Article history:
Received 21 July 2014
Received in revised form
26 September 2014
Accepted 7 October 2014
Available online 17 October 2014

Keywords:
Near-infrared quantum dots
CdTe/CdS@ZnS–SiO_2
Hg^{2+}
Label-free detection
Imaging

ABSTRACT

Highly luminescent, good stable and low toxic N-acetyl-L-cysteine (NAC) capped CdTe/CdS@ZnS–SiO_2 near-infrared (NIR)-emitting quantum dots (QDs) were successfully fabricated in aqueous solution *via* a microwave irradiation reduction route, in which thiol-capped CdTe/CdS QDs were employed as core templates and $ZnCl_2$, NAC and tetraethyl orthosilicate as shell precursors. This presented ZnS-like clusters filled hybrid SiO_2 model not only greatly improved the brightness and stability of original CdTe/CdS QDs, but also tremendously decreased the cytotoxicity towards HeLa cells. Furthermore, it was found that Hg^{2+} could effectively selective quench the QD NIR emission based on electron transfer process. On the basis of this fact, a simple, rapid and specific method for trace Hg^{2+} determination was proposed. Under optimal conditions, the fluorescence intensity decreased linearly with the concentration of Hg^{2+} ranging from 5.0×10^{-9} to 1.0×10^{-6} M and the limit of detection for Hg^{2+} was 1.0×10^{-9} M ($S/N = 3$). As practical applications, the novel NIR sensor has been demonstrated to monitor and image Hg^{2+} level in milk power and HeLa cells respectively with satisfactory results obtained.

1. Introduction

Near-infrared (NIR) fluorescence-based bio-sensor and -imaging applications have significantly contributed to diagnostic and biomedical fields because at the NIR wavelength (650–900 nm) light has deep tissue penetration and induces minimal autofluorescence [1–4]. In comparison with organic dye, semiconductor nanocrystals (quantum dots, QDs) as one kind of the most promising NIR lumophores have been widely studied in the past decade benefiting from their unique size-tunable optical properties [5]. In spite of their widespread use, the QD-based NIR fluorescence techniques have remained a challenging research objective due to the following reasons: (1) the most routine preparation of NIR-emitting QDs through high-temperature organometallic approaches may involve relatively complicated multistep processes and intrinsic hydrophobic property restricted their direct applications in biosystems [6,7]. On the other hand, when using aqueous methods, almost the obtained NIR-emitting QDs have inferior luminescence efficiency due to the poor nucleation environment [8–11]. (2) For application the water-soluble thiols play an important role and contribute greatly to the stability and functionality of the resulting QDs [12]. Unfortunately, these QDs are readily subjected to the photo-oxidation and photo-bleaching when used to sensing in complex biological media such as living cells [13]. (3) QDs are difficult to functionalize in a controlled manner and the release of heavy metal ions from the particle surface produces potential cytotoxicity [14,15].

Thus it can be seen that the surface structure of QDs seriously affect the nature of these nanocrystals, thereby hindering their further developments in active fields. Recently, epitaxial growth of an inorganic shell (mainly including CdS, ZnS, CdSe and SiO_2) on the surface of initial QD cores to prepare core/shell QDs has been explored for improving the quality of visible-emitting QDs in aqueous solution [16–18]. Among these core/shell structures, SiO_2 is one superior hydrophilic coating layer regarding their high stability, good biocompatibility and convenient processability in aqueous media [19,20]. Nevertheless, the existence of a SiO_2 shell has its own limitation such as the decrease of fluorescence intensity [21,22]. To solve this problem, Yang and Murase first presented the fabrication of hybrid SiO_2-coated CdTe nanocrystals [23]. In this model, a hybrid SiO_2 shell with CdS-like clusters was formed on a CdTe core. The SiO_2 layer prevented a lattice constant mismatch between the

* Corresponding author. Tel.: +86 27 87282043; fax: +86 27 87282043.
E-mail address: hyhan@mail.hzau.edu.cn (H. Han).

http://dx.doi.org/10.1016/j.snb.2014.10.031
0925-4005/

core and clusters, while the CdS-like clusters donated energy to the core, resulting in the improvement of fluorescence efficiency. In order to further decrease the toxicity of Cd^{2+}, Zhu and co-workers recently reported the preparation of ZnS-like clusters filled hybrid SiO_2-coated CdSeTe QDs *via* a microwave-assisted approach [24]. The obtained CdSeTe@ZnS–SiO_2 QDs possessed higher fluorescence and lower cytotoxicity, and have been successfully applied in the detection of Cu^{2+}. However, to our knowledge, the high-quality water-soluble NIR-emitting QDs have remained elusive, despite pioneering efforts devoted to the rational modification of visible-emitting QDs.

Much attention has been paid to the development of fluorescent sensors for the rapid, sensitive and selective detection of chemically and biologically significant ionic species. Mercury, is considered highly toxic and widespread pollutant, and it exists in a variety of different forms (metallic, ionic, and as a part of organic salts and complexes) [25]. Mercuric ion (Hg^{2+}), as one of the most stable inorganic forms of mercury, can accumulate in organisms and interact with the thiol groups in protein to cause serious threat to human health and natural environment [26]. Therefore, development of fluorescent Hg^{2+} probes is of vital importance. Up to now, a variety of fluorescent chemodosimeters for trace amounts of Hg^{2+} detection have been developed and mainly located in the UV and visible range [27–33]. To develop the application of Hg^{2+}-selective fluorescent sensors in complex biological systems, NIR fluorescent nanosensors should be a more suitable and reliable choice because the fact that the NIR window it offers in the sensor design of lower background interference, and commonly leading a wider linear range and lower detection limit. However, the reports concerning Hg^{2+} fluorescent nanoprobes reliant on NIR emission were rather rare [34,35].

With these insights, here we have presented the design and preparation of ZnS-like clusters filled hybrid SiO_2-coated CdTe/CdS NIR-emitting QDs. As shown in Scheme 1, the mercaptopropionic acid (MPA)-capped NIR-emitting CdTe/CdS QDs was first synthesized using a previous hydrothermal method with small changes [36]. Then, the CdTe/CdS QDs were coated with a very thin SiO_2 shell containing Zn^{2+} and N-Acetyl-L-cysteine (NAC) molecules in an alkaline condition. In this case, NAC was selected as the precursors of ZnS and the later stabilizers of QDs. It is worth mentioning

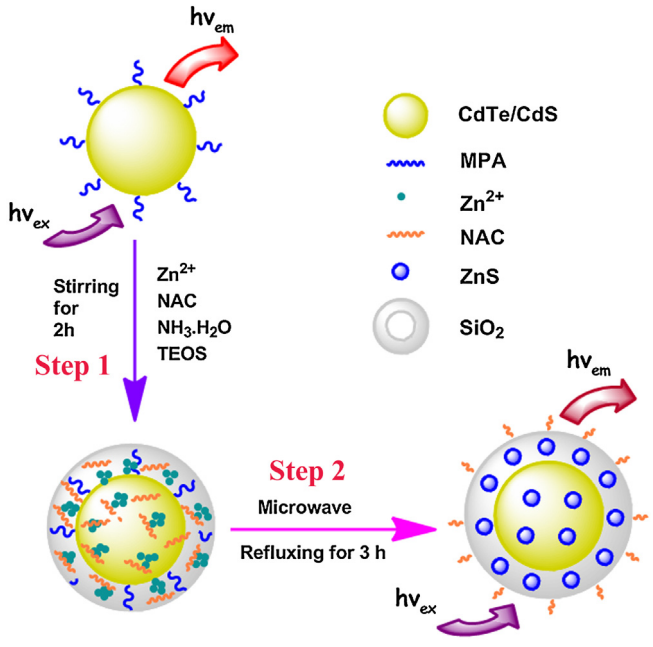

Scheme 1. Schematic illustration for the preparation of CdTe/CdS@ZnS–SiO_2 QDs.

that NAC as alternative stabilizers of MPA for NIR-emitting QDs that are safer and more environmentally friendly, which are beneficial to decrease the toxicity [36]. After that, the SiO_2 coated QDs were refluxed under microwave irradiation. Compared with CdTe/CdS QDs, the obtained CdTe/CdS@ZnS–SiO_2 QDs possessed higher NIR fluorescence, stronger stability and lower cytotoxicity. Furthermore, we found that the NIR fluorescence of QDs can be selectively quenched by Hg^{2+} based on electron transfer process. These QDs have been demonstrated to accord with demands for the nanoprobes of NIR in detecting and imaging of trace Hg^{2+} in milk powder and living cells, respectively.

2. Materials and methods

2.1. Reagents

All the starting materials of the CdTe/CdS and CdTe/CdS@ZnS–SiO_2 NIR-emitting QDs synthesis were used without further purification. $CdCl_2{\cdot}2.5H_2O$ (99.0%), $NaBH_4$ (96.0%), tellurium powder (99.9%) and $ZnCl_2$ were obtained from Sinopharm Chemical Regent Co. Ltd. (Shanghai, China). Tetraethoxysilane (TEOS), N-Acetyl-L-cysteine (NAC), mercaptopropionic acid (MPA, 99%), 3-(4,5-dimethylthiazol-2-yl)-2,5-diphenyl tetrazolium bromide (MTT) and dimethylsulfoxide (DMSO) were purchased from Sigma–Aldrich Chemicals Co. Mercury nitrate ($Hg(NO_3)_2$) and other common solvents and salts were obtained from Aladdin Regent Co. Ltd. For all aqueous solutions, high-purity ultrapure water from a Millipore (18.2 MΩ cm) system was used throughout the experiments.

2.2. Experimental measurements

The optical absorption spectra were acquired on the Nicolet Evolution 300 UV–vis spectrometer (Thermo, USA) coupled with a 1.00 cm quartz cell. Fluorescence spectra and fluorescence lifetime study were performed on an Edinburgh FLS920 spectrometer (Edinburgh Instruments Ltd., UK) with an integrating-sphere attachment under excitation of 380 nm. The quantum yield (QY) of CdTe/CdS and CdTe/CdS@ZnS–SiO_2 QDs were calculated according to reported procedure, using Rhodamine 6G in ethanol as a standard (QY = 95%). Fourier-transform infrared (FT-IR) spectra were collected on a Nicolet Avatar-330 spectrometer (Thermo, USA) with 4 cm^{-1} resolution using the KBr pellet technique. Fluorescence microscopy images were carried out with inverted fluorescence microscope (Eclipse Ti, Nikon). X-ray photoelectron spectroscopy (XPS) data were measured using VG Multilab 2000 X-ray photoelectron spectrometer. High-resolution transmission electron microscopy (HRTEM) images were acquired using a FEI Tecnai G20 transmission electron microscope (FEI, USA) operating at an acceleration voltage of 200 kV. Measurements of hydrodynamic diameters of the QDs in aqueous solution were acquired on a Zetasizer Nano-ZS90 (Malvern Instruments Ltd., UK). The concentration analyses of Hg^{2+} in practical samples were carried out on a AFS-830 cold-vapor atomic fluorescence spectrophotometer (CV-AFS). Microwave reactions were carried out using an APEX microwave chemical reactor.

2.3. Preparation of NIR-emitting NAC-capped CdTe/CdS@ZnS–SiO_2 QDs

NIR-emitting MPA-capped CdTe/CdS QDs were first prepared through a hydrothermal approach described previously with small modifications [36] (Supporting Information). The CdTe/CdS@ZnS–SiO_2 QDs were prepared using a two-step synthesis process shown in Scheme 1. In step 1, the CdTe/CdS QDs were coated with a thin SiO_2 layer at room temperature through

a StÖber method. Typically, ammonia aqueous solution (70 μL, 20%), tetraethoxysilane (TEOS, 400 μL), Zn^{2+} (0.1 M, 100 μL) and NAC (0.1 M, 200 μL) were successively added into the purified CdTe/CdS solution (10 mL, pH 10.5). After being stirred at room temperature for 2 h, the CdTe/CdS were coated with a thin SiO_2 layer containing Zn^{2+} and NAC. In step 2, a microwave-assisted reflux process (200 W, 3 h) using this solution caused ZnS-like clusters to nucleate and grow in the SiO_2 shell. The resulting products were purified using 30 kD ultrafiltration centrifuge tube. The CdTe/CdS@ZnS–SiO_2 QDs were dried overnight at room temperature in a vacuum. The final product in powder form could be resuspended in ultrapure water.

2.4. Near-infrared fluorescence assay for Hg^{2+}

Mercury nitrate ($Hg(NO_3)_2$) aqueous solution was used for the determination of Hg^{2+}. To a 2 mL calibrated test tube 100 μL 1.0×10^{-7} M the purified CdTe/CdS@ZnS–SiO_2 QD solution and certain amounts of Hg^{2+} were sequentially added. The mixture was then diluted to volume with 0.01 M phosphate buffer solution (PBS, pH 7.4) and mixed thoroughly. Two minutes later, the mixture was transferred to a 3 mL cuvette and the fluorescence intensity of solution was recorded at 677 nm with the excitation wavelength of 380 nm.

2.5. Hg^{2+} detection in milk powder sample

The milk power sample was first accurately weighted (0.1000 g) and digested with a mixture (1 mL) of concentrated nitric acid and hydrogen peroxide (3:1), then heated under the microwave radiation until the solution became clear. Afterwards, the solution was diluted with water (10 mL) and the pH was adjusted to 7.4. For a typical detection, 100 μL sample solution, 100 μL QD solution and different Hg^{2+} were mixed in 0.01 M PBS (total volume: 2 mL). The subsequent fluorescence measurement procedures were the same as above.

2.6. Hg^{2+} imaging in Hela cells

The Hela cells were cultured in six-well plates with DMEM with 10% fetal bovine serum to obtain a suitable density (70–80% confluence). The complete DMEM was removed, and the cells were then suspended in PBS (pH 7.4). To image Hg^{2+}, cells were washed with PBS (pH 7.4) three times. The QD solution was first added to the culture dish, after that, different amounts of Hg^{2+} were added to the same culture dish and incubated for different times. Finally, the culture dish was observed under the inverted fluorescence microscope at different moments.

3. Results and discussion

3.1. Preparation and characterization of NIR-emitting CdTe/CdS@ZnS–SiO_2 QDs

The fabrication procedure and condition of CdTe/CdS@ZnS–SiO_2 QDs are schematically illustrated in Scheme 1. Briefly, the MPA-capped NIR-emitting CdTe/CdS QDs were first prepared and purified. Afterwards, the CdTe/CdS QDs were coated with a thin silica layer at room temperature in the presence of Zn^{2+} and NAC (Step 1). It is worth noting that Zn^{2+} and NAC were the precursors of ZnS-like clusters, because Zn^{2+} can gradually incorporate with S^{2-} released from the gradual thermal decomposition of NAC. Finally, the hybrid SiO_2-coated QDs were obtained *via* a reflux process under microwave irradiation (Step 2).

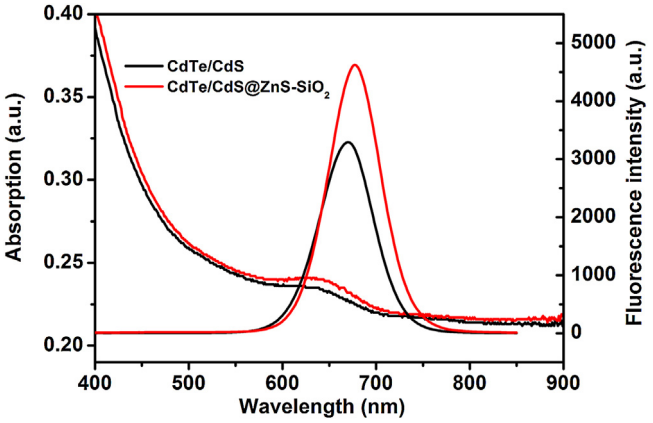

Fig. 1. UV–vis absorption (left) and fluorescence spectra (right) of CdTe/CdS and CdTe/CdS@ZnS–SiO_2 QD.

Fig. 1 demonstrates the typical absorption and fluorescence spectra of CdTe/CdS and corresponding CdTe/CdS@ZnS–SiO_2 QDs. After the reflux was finished, the absorption peak of CdTe/CdS@ZnS–SiO_2 QDs was slightly red-shifted, which could be due to the increase in the size of QDs. This phenomenon was also observed in fluorescence spectra. On the other hand, the fluorescence intensity was significantly enhanced after the reaction. The main factor contributing to the increased efficiency in this case may be the absence of an interface between CdTe/CdS core and ZnS-like clusters. Since the clusters were not chemically bonded to the core surface due to the separation of the SiO_2 layer, thus the lattice constant mismatch was avoided, leading to the fluorescence enhancement through the effect of long-range resonance transfer (LRRT) [37,38]. Representative HRTEM images of the as-synthesized QDs samples are shown in Fig. 2(A, B). The nanoparticles were nearly monodisperse, and the mean sizes of CdTe/CdS QDs were about 5.3 nm, after coating with a ZnS–SiO_2 shell, the average sizes increased to about 6.8 nm, indicating the thick of ZnS–SiO_2 shell was about 0.8 nm (inset). Meanwhile, we could not find any fault interface in lattice fringe after coating, implying that alloyed structure is not formed in the whole process [39]. Comparatively, the corresponding hydrodynamic diameters of the QDs in water are presented in Fig. S1 (Supporting Information). The average hydrodynamic diameters of CdTe/CdS QDs in aqueous solution were 9.7 nm, and CdTe/CdS@ZnS–SiO_2 QDs were 26.9 nm, slightly larger than the CdTe/CdS QDs. The difference in diameter measured by HRTEM and dynamic light scattering (DLS) is attributed to different surface species of the as-prepared QDs in aqueous phase.

The FTIR spectra were used to identify the functional group on the surface of the CdTe/CdS@ZnS–SiO_2 QDs. In Fig. 2C, the FTIR spectrum of NAC capped CdTe/CdS@ZnS–SiO_2 QDs was similar to that of pure NAC. In both samples, the characteristic peak at 1641 cm^{-1} corresponds to the C=O vibration, which represents the carboxyl group. Furthermore, the peak at 1398 cm^{-1} was attributed to C–N group, the peak at 968 cm^{-1} was attributed to the N–H group, and the peak at 1554 cm^{-1} corresponded to R-CO-NHR. The strong peak at 1117 cm^{-1} was ascribed to the silica capping on CdTe/CdS@ZnS–SiO_2 QDs. The diminution of the broad absorption around 2550 cm^{-1} resulting from the S–H bond in the NAC molecule indicated that the thiol group of NAC combined on the surface of the CdTe/CdS@ZnS–SiO_2 QDs through the Cd–S bond. All the results indicated that NAC was capped on the surface of hybrid SiO_2-coated QDs. Further evidence on the surface structure of QDs can be obtained from the XPS analysis. As shown in Fig. 2D, compared with the original CdTe/CdS QDs, the emergence of new Zn2p and Si (2p, 2s) peaks in the CdTe/CdS@ZnS–SiO_2 QDs were attributed to Zn and Si from the ZnS and SiO_2 respectively, and the

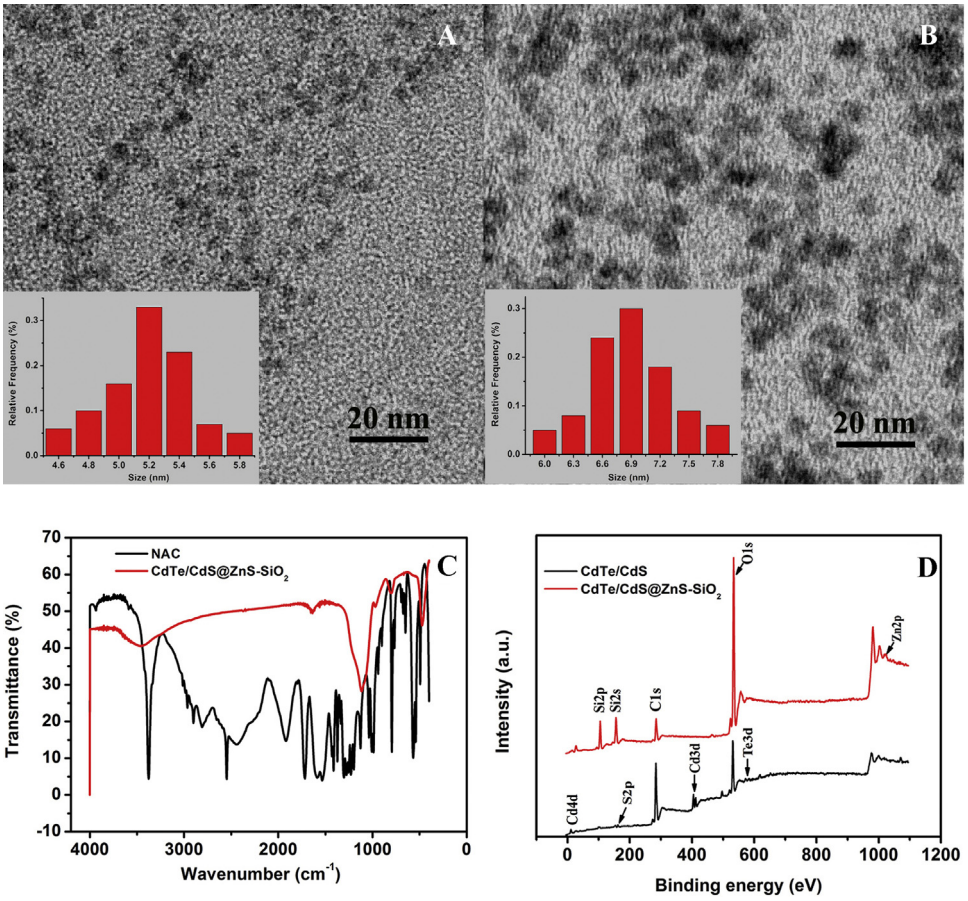

Fig. 2. HRTEM photograph of CdTe/CdS (A) and CdTe/CdS@ZnS–SiO_2 (B) QDs. FTIR spectra (C) of NAC and CdTe/CdS@ZnS–SiO_2 QDs. XPS (D) of the prepared CdTe/CdS and CdTe/CdS@ZnS–SiO_2 QDs.

higher content of O as well as the lower content of Cd, Te, S and C indicated the formation of ZnS-like clusters filled hybrid SiO_2 shell.

3.2. Stability of CdTe/CdS@ZnS–SiO_2 QDs

As previously reported, mercapto carboxylic acid modified QD colloidal solutions were not stable for a long time when they were precipitated and redispersed in ligand-free ultrapure water or buffer solutions, especially under the condition of low concentration [13]. This is because mercapto small molecules could fall off from the surface of the QDs readily, resulting in the agglomeration of the nanoparticles, and consequently the red-shift of emission spectrum and the decrease of fluorescence intensity [40]. Based on this, the colloidal stability of the CdTe/CdS and CdTe/CdS@ZnS–SiO_2 QD solutions was investigated. As shown in Fig. 3A, it was observed that the emission intensity of CdTe/CdS QDs reduced successively with the increasing of store time at a low concentration (5 nM). Meanwhile, the spectral wavelength maximum was also red-shifted about 15 nm after 3 h. Oppositely, there were no obvious changes concerning the emission intensity and wavelength maximum of CdTe/CdS@ZnS–SiO_2 QDs, indicating the effective protection of surface states by ZnS–SiO_2 shell [24]. It is worth mentioning that the concentration of QDs has a significant influence on the sensitivity of fluorescence detection. In general, the lower of the concentration, the lower of detection limit, and vice versa. Here, we chose 5 nM as experimental concentrations of QDs, which was much lower than the same type of QD-based fluorescent probes.

We further evaluated the photostability of the as-prepared QDs. Fig. 3B shows that the fluorescence of CdTe/CdS QDs dropped to 80% of the original fluorescence intensity in 3 h. In contrast, the fluorescence of the CdTe/CdS@ZnS–SiO_2 QDs was remarkably stable and decreased only slightly under UV irradiation retaining >90% of the original intensity after irradiation for 3 h. This comparison indicates a superior photostability of the CdTe/CdS@ZnS–SiO_2 QDs which makes their use for long-term and real-time bioassay and bioimaging applications possible [5]. Additionally, the influence of pH in a range between 4.0 and 10.0 was studied in order to select the optimal conditions for the determination. As illustrated in Fig. 3C, the effect of pH on the CdTe/CdS@ZnS–SiO_2 QDs suggested that the QDs were pH-dependent, due to the protonation and deprotonation of the surface binding thiolates (NAC) [41]. The optimal fluorescence intensity was obtained at the vicinity of pH 8.0. In order to adapt to the pH of physical environment, 0.01 M of PBS (pH 7.4) was recommended for used in the following work.

3.3. Sensing performance of NAC-capped CdTe/CdS@ZnS–SiO_2 QDs for Hg^{2+}

We explored the feasibility of using such hybrid SiO_2-coated QDs for Hg^{2+} detection. It was seen that CdTe/CdS@ZnS–SiO_2 QD solution in the absence of Hg^{2+} exhibited a strong NIR fluorescence peak at 677 nm (Fig. 4A, curve a) and its fluorescence QY was determined to be 45.8%, in comparison with rhodamine 6G in ethanol (QYs: 95%) [42]. In contrast, the presence of Hg^{2+} led to an obvious decrease of fluorescence in intensity, indicating that Hg^{2+} could effectively quench the fluorescence of QDs (Fig. 4A, curve b and c). Fig. 4B reveals the influence of the reaction time on the luminescence of QDs. The reaction between NAC-capped CdTe/CdS@ZnS–SiO_2 QDs and Hg^{2+} was completed within 2 min

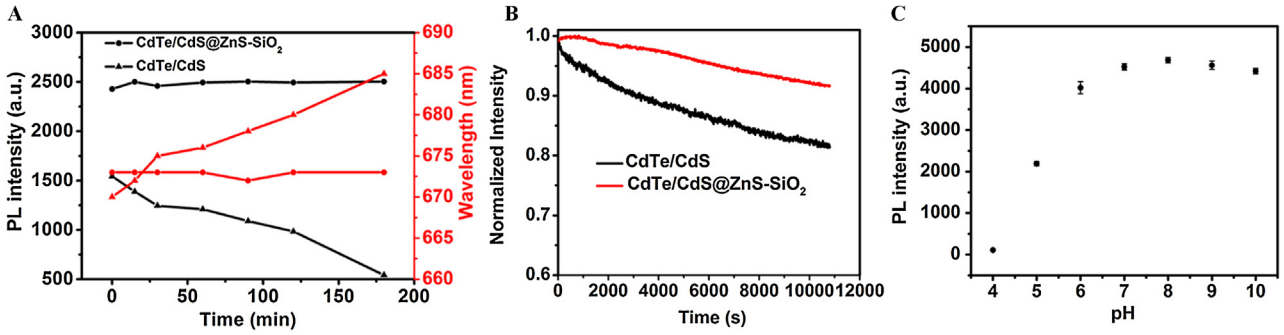

Fig. 3. Colloidal stability (A) and photostability (B) of the prepared CdTe/CdS (triangle) and CdTe/CdS@ZnS–SiO_2 (dots) QDs. Fluorescence intensity (C) of the CdTe/CdS@ZnS–SiO_2 QDs in PBS (10 mM) at different pH values, the concentration of QDs is 5 nM.

and the fluorescence signals were stable for more than 2 h. For a sensitivity study, different concentrations of Hg^{2+} in the range of $0 \sim 2.5 \times 10^3$ nM were investigated. Fig. 4C shows a gradual decrease in fluorescence intensity at 677 nm with an increased Hg^{2+} concentration, and the fluorescence was quenched completely when the concentration of Hg^{2+} solution reached 2.5 μM. The fluorescence quenching data follows the Stern–Volmer equation (Fig. 4D): $F_0/F = 1.18823 + 0.00211C_0$. Where C_0 is the analyte (Hg^{2+}) concentration, and F_0, F are the fluorescence intensities of the resulting CdTe/CdS@ZnS–SiO_2 QDs in the absence and presence of Hg^{2+}. The F_0/F response to Hg^{2+} concentration indicated a nearly linear behavior ($R^2 = 0.995$) in the range from 5 nM to 1 μM. The limit of detection is estimated to be 1 nM at a signal-to-noise ratio of 3, which is much lower than the tolerance limit of 2 ppb (10×10^{-9} M) for mercury in drinking water permitted by the United States Environmental Protection Agency (EPA) [43]. Furthermore, a comparison of the proposed nanosensor with some other assays for the determination of Hg^{2+} is made as shown in Table S1 (Supporting Information). Although the results showed that some sophisticated analytical techniques (CVAAS and voltammetry) had a lower detection limit, our proposed method for Hg^{2+} is low cost and the selectivity is superior. Most importantly, compared with other fluorescent probes in the visible range, the fabricated nanosensor displayed a wider linear detection range and lower detection limit.

3.4. Possible mechanism of quenching

To date, two mechanisms containing electron transfer process and ion binding interaction have been proposed to explain the quenching effect of Hg^{2+} on QD fluorescence [44]. In our study, we speculated Hg^{2+} could quench the fluorescence of CdTe/CdS@ZnS–SiO_2 QDs mainly *via* electron transfer. As depicted in Fig. 5A, no shift was observed in the absorption peak of CdTe/CdS@ZnS–SiO_2 QDs with addition of 0.5 μM Hg^{2+}, indicating the effective barrier effect of hybrid ZnS–SiO_2 shell for metal

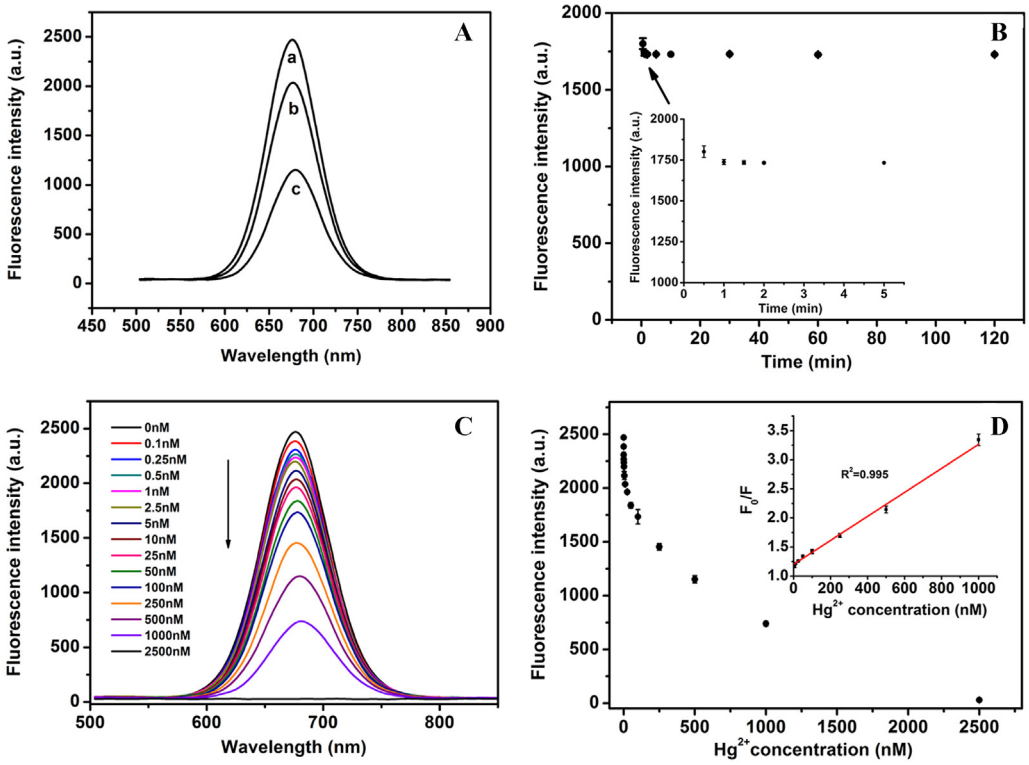

Fig. 4. Fluorescence intensity (A) of the CdTe/CdS@ZnS–SiO_2 QDs at different concentrations of Hg^{2+} (a: 0 M, b: 10 nM, c: 500 nM). Time-dependent fluorescence response (B) of the CdTe/CdS@ZnS–SiO_2 QDs to Hg^{2+} (100 nM). Fluorescence emission spectra (C) of CdTe/CdS@ZnS–SiO_2 QDs in the presence of different concentrations of Hg^{2+}. The linear relation (D) between the fluorescence intensity of CdTe/CdS@ZnS–SiO_2 QDs and the Hg^{2+}concentration.

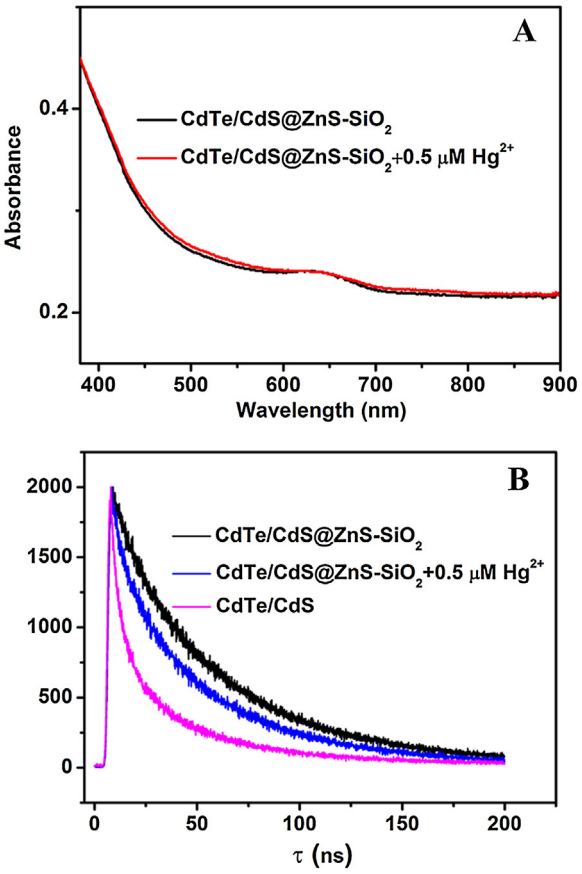

Fig. 5. UV–vis absorption spectra (A) of the CdTe/CdS@ZnS–SiO_2 QDs and CdTe/CdS@ZnS–SiO_2 QDs in the presence of 0.5 μM Hg^{2+}. Fluorescence decay curves (B) of CdTe/CdS, CdTe/CdS@ZnS–SiO_2, and CdTe/CdS@ZnS–SiO_2 after adding 0.5 μM Hg^{2+} (λ_{ex} = 380 nm, measured at the maximum of the fluorescence).

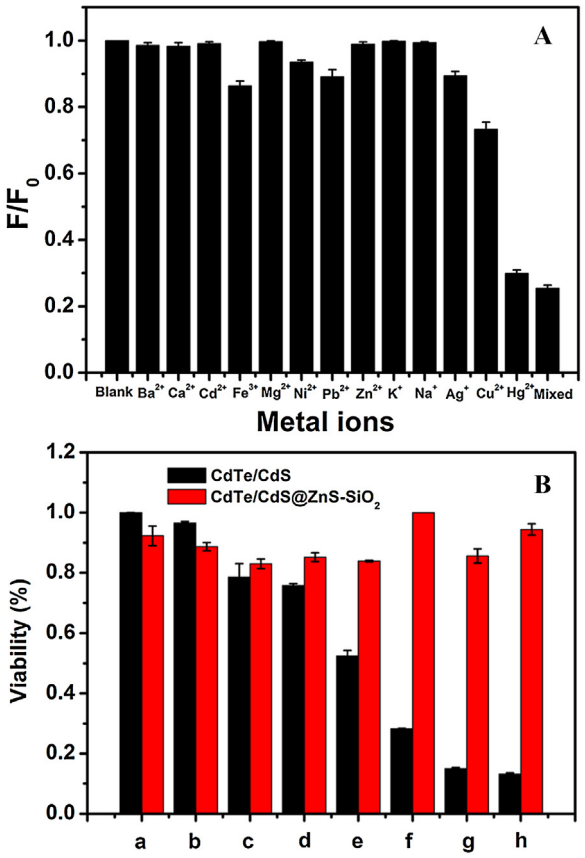

Fig. 6. Relative fluorescence (A) of CdTe/CdS@ZnS–SiO_2 QDs solution in the presence of different concentrations of various metal ions (Hg^{2+}: 1 μM, Cu^{2+}: 5 μM, Ca^{2+}: 100 μM, other: 10 μM). F_0 and F correspond to the fluorescence intensity of CdTe/CdS@ZnS–SiO_2 QDs in the absence and presence of various metal ions. Cytotoxicity (B) of CdTe/CdS and CdTe/CdS@ZnS–SiO_2 QDs with different concentrations and incubation for 24 h with HeLa cells, (a) blank, (b) 5, (c) 10, (d) 50, (e) 100, (f) 500, (g) 1000, (h) 5000 (nM).

cations. In addition, there was also no spectra shift in fluorescence spectra although the fluorescence intensity of QDs was quenched at the presence of Hg^{2+} (Fig. 4C). To further verify the quenching effect, the fluorescence decays were examined. As shown in Fig. 5B, the decay curves of all the samples can be well fitted to a biexponential model described by $F(t) = A + B_1\exp(-t/\tau_1) + B_2\exp(-t/\tau_2)$ [45]. The average lifetimes of CdTe/CdS QDs was 41 ns, which was much lower than that of CdTe/CdS@ZnS–SiO_2 QDs (56 ns), suggesting the hybrid ZnS–SiO_2 shell effectively decreased the non-radiative decay channel. After addition of Hg^{2+}, the fluorescence lifetime was reduced to 51 ns, which may result from the ultrafast electron transfer from QDs to Hg^{2+} [46].

3.5. Effect of foreign ions

Besides sensitivity, selectivity is another important parameter to evaluate the performance of the sensing system. Therefore, the quenching effect in the presence of representative 12 kinds of cations under the same conditions was investigated. As revealed in Fig. 6A, Hg^{2+} (1 μM) displayed the strongest fluorescence quenching and Cu^{2+} (5 μM) could minimally quench the fluorescence, while other high concentrations of ions (Ca^{2+}: 100 μM, Fe^{3+}, Zn^{2+}, Cd^{2+}, Mg^{2+}, Ni^{2+}, Pb^{2+}, K^+, Na^+, Ag^+: 10 μM) scarcely had effect on the fluorescence of CdTe/CdS@ZnS–SiO_2 QDs. It was worth mentioning that previous reports showed Cu^{2+} have strong quenching effect on the Cd-based QDs. But in this case, this quenching effect can be effectively reduced because the thin hybrid SiO_2 shell layer effectively prevented the binding of Cu^{2+} onto the QDs. Furthermore, this nanoprobe still demonstrated an excellent selectivity in the presence of all possible interference ions.

3.6. Cytotoxicity of NAC-capped CdTe/CdS@ZnS–SiO_2 QDs

As another critical characteristic for biological applications, the cytotoxicity of CdTe/CdS QDs and CdTe/CdS@ZnS–SiO_2 QDs were elaborately studied with MTT viability assay (Supporting Information). As displayed in Fig. 6B, the cell lines maintained greater than 80% cell viability after 24 h of treatment with CdTe/CdS@ZnS–SiO_2 QD at concentrations range from 5 nM to 5 μM, while the cell viability incubated with CdTe/CdS QDs dropped to only 50% at the concentration of 100 nM, and became negligible after addition 5 μM of QDs. This fact should be ascribed to the low toxicity of the shell. The cross-linked ZnS–SiO_2 shell greatly protected the QDs from photobleaching, meanwhile the ZnS cluster layer has less susceptibility to oxidation than the bare CdTe/CdS core [24]. To our knowledge, MPA is the common stabilizer used in synthesizing NIR-emitting QDs but it is a volatile liquid with an awful odor and carcinogenic properties [36]. Here, NAC was selected for growth of ZnS cluster and as stabilizer for QDs, because NAC is a therapeutic drug used as a mucolytic reagent and in the treatment of acetaminophen hepatotoxicity, and is of interest for antioxidant/radical-scavenging activity [47]. All of these results demonstrated that our QDs possessed the capability for the biological applications.

Table 1
Direct determination of Hg^{2+} content in three milk powder samples using the proposed sensors.

Sample	Added Hg^{2+} concentration (nM)	Found Hg^{2+} concentration (nM)		Recovery	RSD ($n = 5$)
		This method	CV-AFS		
1	2.5	2.7	2.6	108.0%	3.5%
2	25.0	26.4	25.3	105.6%	4.6%
3	100.0	102.2	100.4	102.2%	2.3%

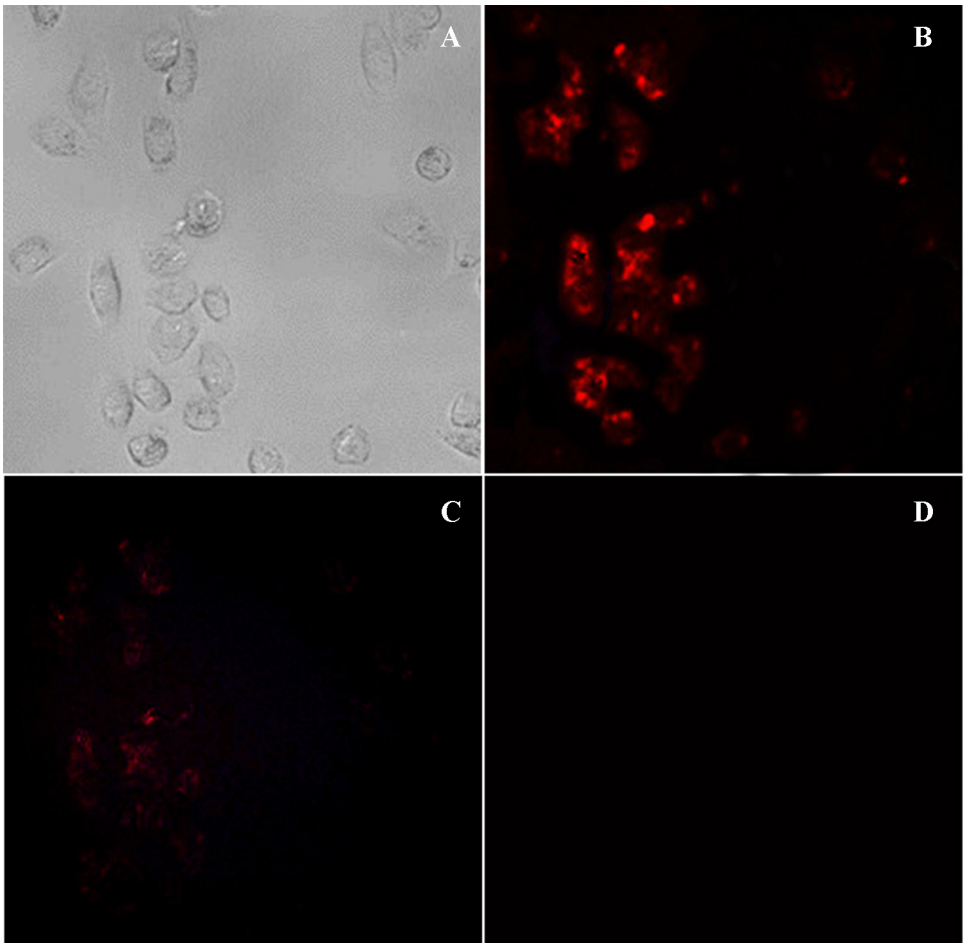

Fig. 7. Fluorescence microscopic images of living HeLa cells: (A) cells supplemented with CdTe/CdS@ZnS–SiO_2 QDs for 30 min under visible light, (B) cells supplemented with the CdTe/CdS@ZnS–SiO_2 QDs for 30 min and further addition different concentrations of Hg^{2+} (C: 0.5 μM, D: 2.5 μM) under the excitation wavelength of 380 nm.

3.7. Analytical applications

Taking advantage of NIR emission wavelength sensing ability, the detecting of Hg^{2+} in milk power was first carried out, in which no fluorescence background was observed in the NIR region with excitation at 380 nm. After pretreatment (experiment section), the resultant samples were spiked with standard solutions containing different concentrations of Hg^{2+}. Table 1 describes the results of three independent milk power samples obtained using the proposed fluorescence probes. It was seen that the results of recovery for the three samples were in the range of 102.2–108.0%, which was satisfactory for quantitative assays performed in biological samples. Besides, the proposed method determination results were in a good agreement with the results obtained by CV-AFS suggesting that the method is reliable and practical.

Next, we applied the QD probe to monitor the concentration of Hg^{2+} in living cells. After CdTe/CdS@ZnS–SiO_2 QDs were added and incubated for 30 min, intense deep red fluorescence can be observed in the cytosol of the cell under the inverted fluorescent microscope with the excitation wavelength of 380 nm (Fig. 7B). The bright field imaging showed (Fig. 7A) the clear contour of the cells, which indicated that most of the cells were adherent cells and viable throughout the imaging experiments [48]. When 0.5 μM Hg^{2+} was supplemented to cells and incubated for another 5 min, a distinct decrease of the fluorescence intensity can be seen in Fig. 7C. When the concentration of Hg^{2+} was increased to 2.5 μM, no fluorescence can be seen (Fig. 7D). All of the phenomena showed that these NIR fluorescence probes could be used in the detection of Hg^{2+} in complex biological samples.

4. Conclusion

In summary, coating of ZnS-like clusters filled hybrid SiO_2 shell has been proven to be an effective strategy for producing high-quality NIR-emitting QDs in aqueous solution for the first time. The as-prepared CdTe/CdS@ZnS–SiO_2 QDs showed strong NIR emission, excellent colloidal- and photo- stability, low toxicity and good water solubility. Such QDs have been further used as a

novel sensing probe for label-free, sensitive detection of Hg^{2+} with a detection limit as low as 1 nM. This sensing system also possessed high selectivity toward Hg^{2+} analysis and has been successfully used for the detecting and imaging of trace Hg^{2+} in milk powder and living cells, respectively. Our present study allows upward scalability in terms of fabrication of fluorescent and biocompatible nanoparticles which could be applied in biosensing and imaging.

Acknowledgments

We gratefully acknowledge the financial support from National Natural Science Foundation of China (21375043, 21175051 and 21405139), and scientific research start-up funding of Zhejiang University of Technology (101010629).

Appendix A. Supplementary data

Supplementary data associated with this article can be found, in the online version, at http://dx.doi.org/10.1016/j.snb.2014.10.031.

References

[1] S. Kim, Y.T. Lim, E.G. Soltesz, A.M. De Grand, J. Lee, A. Nakayama, J.A. Parker, T. Mihaljevic, R.G. Laurence, D.M. Dor, Near-infrared fluorescent type II quantum dots for sentinel lymph node mapping, Nat. Biotechnol. 22 (2003) 93–97.
[2] S. Zhang, V. Metelev, D. Tabatadze, P.C. Zamecnik, A. Bogdanov, Fluorescence resonance energy transfer in near-infrared fluorescent oligonucleotide probes for detecting protein-DNA interactions, Proc. Natl. Acad. Sci. U.S.A. 105 (2008) 4156–4161.
[3] A.M. Smith, M.C. Mancini, S. Nie, Second window for in vivo imaging, Nat. Nanotechnol. 4 (2009) 710.
[4] Y. Xia, L. Song, C. Zhu, Turn-on and near-infrared fluorescent sensing for 2, 4, 6-trinitrotoluene based on hybrid (gold nanorod)-(quantum dots) assembly, Anal. Chem. 83 (2011) 1401–1407.
[5] X. Michalet, F. Pinaud, L. Bentolila, J. Tsay, S. Doose, J. Li, G. Sundaresan, A. Wu, S. Gambhir, S. Weiss, Quantum dots for live cells, in vivo imaging, and diagnostics, Science 307 (2005) 538–544.
[6] S. Kim, B. Fisher, H.-J. Eisler, M. Bawendi, Type-II quantum dots: CdTe/CdSe(core/shell) and CdSe/ZnTe(core/shell) heterostructures, J. Am. Chem. Soc. 125 (2003) 11466–11467.
[7] H. Seo, S.-W. Kim, In situ synthesis of CdTe/CdSe core-shell quantum dots, Chem. Mater. 19 (2007) 2715–2717.
[8] L. Zou, Z. Gu, N. Zhang, Y. Zhang, Z. Fang, W. Zhu, X. Zhong, Ultrafast synthesis of highly luminescent green- to near infrared-emitting CdTe nanocrystals in aqueous phase, J. Mater. Chem. 18 (2008) 2807–2815.
[9] Y. Zhang, Y. Li, X.-P. Yan, Aqueous layer-by-layer epitaxy of type-II CdTe/CdSe quantum dots with near-infrared fluorescence for bioimaging applications, Small 5 (2008) 185–189.
[10] W. Mao, J. Guo, W. Yang, C. Wang, J. He, J. Chen, Synthesis of high-quality near-infrared-emitting CdTeS alloyed quantum dots via the hydrothermal method, Nanotechnology 18 (2007) 485611.
[11] G.-X. Liang, M.-M. Gu, J.-R. Zhang, J.-J. Zhu, Preparation and bioapplication of high-quality, water-soluble, biocompatible, and near-infrared-emitting CdSeTe alloyed quantum dots, Nanotechnology 20 (2009) 415103.
[12] W.-S. Zou, D. Sheng, X. Ge, J.-Q. Qiao, H.-Z. Lian, Room-temperature phosphorescence chemosensor and rayleigh scattering chemodosimeter dual-recognition probe for 2,4,6-trinitrotoluene based on manganese-doped ZnS quantum dots, Anal. Chem. 83 (2010) 30–37.
[13] N. Gaponik, D.V. Talapin, A.L. Rogach, K. Hoppe, E.V. Shevchenko, A. Kornowski, A. Eychmüller, H. Weller, Thiol-capping of CdTe nanocrystals: an alternative to organometallic synthetic routes, J. Phys. Chem. B 106 (2002) 7177–7185.
[14] F.M. Winnik, D. Maysinger, Quantum dot cytotoxicity and ways to reduce it, Acc. Chem. Res. 46 (2012) 672–680.
[15] R. Hardman, A toxicologic review of quantum dots: toxicity depends on physicochemical and environmental factors, Environ. Health Perspect. 114 (2006) 165–172.
[16] J.M. Klostranec, W.C. Chan, Quantum dots in biological and biomedical research: recent progress and present challenges, Adv. Mater. 18 (2006) 1953–1964.
[17] A.M. Smith, S. Nie, Semiconductor nanocrystals: structure, properties, and band gap engineering, Acc. Chem. Res. 43 (2009) 190–200.
[18] C.D.M. Donega, Synthesis and properties of colloidal heteronanocrystals, Chem. Soc. Rev. 40 (2011) 1512–1546.
[19] A. Guerrero-Martínez, J. Pérez-Juste, L.M. Liz-Marzán, Recent progress on silica coating of nanoparticles and related nanomaterials, Adv. Mater. 22 (2010) 1182–1195.
[20] Y. Piao, A. Burns, J. Kim, U. Wiesner, T. Hyeon, Designed fabrication of silica-based nanostructured particle systems for nanomedicine applications, Adv. Funct. Mater. 18 (2008) 3745–3758.
[21] T. Nann, P. Mulvaney, Single quantum dots in spherical silica particles, Angew. Chem. Int. Edit. 43 (2004) 5393–5396.
[22] Y. Yang, M.Y. Gao, Preparation of fluorescent SiO_2 particles with single CdTe nanocrystal cores by the reverse microemulsion method, Adv. Mater. 17 (2005) 2354–2357.
[23] P. Yang, N. Murase, Preparation-condition dependence of hybrid SiO_2-coated CdTe nanocrystals with intense and tunable photoluminescence, Adv. Funct. Mater. 20 (2010) 1258–1265.
[24] Y. Shen, L. Li, Q. Lu, J. Ji, R. Fei, J. Zhang, E.S. Abdel-Halim, J.-J. Zhu, Microwave-assisted synthesis of highly luminescent CdSeTe@ZnS–SiO_2 quantum dots and their application in the detection of Cu(II), Chem. Commun. 48 (2012) 2222–2224.
[25] Q. Liu, J. Peng, L. Sun, F. Li, High-efficiency upconversion luminescent sensing and bioimaging of Hg(II) by chromophoric ruthenium complex-assembled nanophosphors, ACS Nano 5 (2011) 8040–8048.
[26] M. Valko, H. Morris, M. Cronin, Metals, toxicity and oxidative stress, Curr. Med. Chem. 12 (2005) 1161–1208.
[27] C.-C. Huang, Z. Yang, K.-H. Lee, H.-T. Chang, Synthesis of highly fluorescent gold nanoparticles for sensing mercury(II), Angew. Chem. Int. Edit. 46 (2007) 6824–6828.
[28] Z.-X. Cai, H. Yang, Y. Zhang, X.-P. Yan, Preparation, characterization and evaluation of water-soluble l-cysteine-capped-CdS nanoparticles as fluorescence probe for detection of Hg(II) in aqueous solution, Anal. Chim. Acta 559 (2006) 234–239.
[29] J. Duan, X. Jiang, S. Ni, M. Yang, J. Zhan, Facile synthesis of N-acetyl-l-cysteine capped ZnS quantum dots as an eco-friendly fluorescence sensor for Hg^{2+}, Talanta 85 (2011) 1738–1743.
[30] W. Lu, X. Qin, S. Liu, G. Chang, Y. Zhang, Y. Luo, A.M. Asiri, A.O. Al-Youbi, X. Sun, Economical, green synthesis of fluorescent carbon nanoparticles and their use as probes for sensitive and selective detection of mercury(II) ions, Anal. Chem. 84 (2012) 5351–5357.
[31] J. Zhang, Y. Zhou, W. Hu, L. Zhang, Q. Huang, T. Ma, Highly selective fluorescence enhancement chemosensor for Hg^{2+} based on rhodamine and its application in living cells and aqueous media, Sens. Actuators B 183 (2013) 290–296.
[32] F. Yan, Y. Zou, M. Wang, X. Mu, N. Yang, L. Chen, Highly photoluminescent carbon dots-based fluorescent chemosensors for sensitive and selective detection of mercury ions and application of imaging in living cells, Sens. Actuators B 192 (2014) 488–495.
[33] C. Guo, J. Irudayaraj, Fluorescent Ag clusters via a protein-directed approach as a Hg(II) ion sensor, Anal. Chem. 83 (2011) 2883–2889.
[34] L. Shang, L. Yang, F. Stockmar, R. Popescu, V. Trouillet, M. Bruns, D. Gerthsen, G.U. Nienhaus, Microwave-assisted rapid synthesis of luminescent gold nanoclusters for sensing Hg^{2+} in living cells using fluorescence imaging, Nanoscale 4 (2012) 4155–4160.
[35] H.-Q. Chen, F. Yuan, S.-Z. Wang, J. Xu, Y.-Y. Zhang, L. Wang, Near-infrared to near-infrared upconverting $NaYF4:Yb^{3+},Tm^{3+}$ nanoparticles-aptamer-Au nanorods light resonance energy transfer system for the detection of mercuric(II) ions in solution, Analyst 138 (2013) 2392–2397.
[36] D. Zhao, Z. He, W.H. Chan, M.M.F. Choi, Synthesis and characterization of high-quality water-soluble near-infrared-emitting CdTe/CdS quantum dots capped by N-Acetyl-l-cysteine via hydrothermal method, J. Phys. Chem. C 113 (2009) 1293–1300.
[37] C. Murray, C. Kagan, M. Bawendi, Synthesis and characterization of monodisperse nanocrystals and close-packed nanocrystal assemblies, Annu. Rev. Mater. Sci. 30 (2000) 545–610.
[38] N. Murase, P. Yang, Anomalous photoluminescence in silica-coated semiconductor nanocrystals after heat treatment, Small 5 (2009) 800–803.
[39] J. Wang, H. Han, Hydrothermal synthesis of high-quality type-II CdTe/CdSe quantum dots with near-infrared fluorescence, J. Colloid Interf. Sci. 351 (2010) 83–87.
[40] Y. Li, L. Jing, R. Qiao, M. Gao, Aqueous synthesis of CdTe nanocrystals: progresses and perspectives, Chem. Commun. 47 (2011) 9293–9311.
[41] M. Gao, S. Kirstein, H. Möhwald, A.L. Rogach, A. Kornowski, A. Eychmüller, H. Weller, Strongly photoluminescent CdTe nanocrystals by proper surface modification, J. Phys. Chem. B 102 (1998) 8360–8363.
[42] L. Qu, X. Peng, Control of photoluminescence properties of CdSe nanocrystals in growth, J. Am. Chem. Soc. 124 (2002) 2049–2055.
[43] Y.-J. Gong, X.-B. Zhang, Z. Chen, Y. Yuan, Z. Jin, L. Mei, J. Zhang, W. Tan, G.-L. Shen, R.-Q. Yu, An efficient rhodamine thiospirolactam-based fluorescent probe for detection of Hg^{2+} in aqueous samples, Analyst 137 (2012) 932–938.
[44] Y.-S. Xia, C.-Q. Zhu, Use of surface-modified CdTe quantum dots as fluorescent probes in sensing mercury (II), Talanta 75 (2008) 215–221.
[45] Q. Zeng, X. Kong, Y. Sun, Y. Zhang, L. Tu, J. Zhao, H. Zhang, Synthesis and optical properties of type II CdTe/CdS core/shell quantum dots in aqueous solution via successive ion layer adsorption and reaction, J. Phys. Chem. C 112 (2008) 8587–8593.
[46] R. van Beek, A.P. Zoombelt, L.W. Jenneskens, C.A. van Walree, C. de Mello Donegá, D. Veldman, R.A.J. Janssen, Side chain mediated electronic contact between a tetrahydro-4H-thiopyran-4-ylidene-appended polythiophene and CdTe quantum dots, Chem. -Eur. J. 12 (2006) 8075–8083.
[47] B. Särnstrand, A. Tunek, K. Sjödin, A. Hallberg, Effects of N-acetylcysteine stereoisomers on oxygen-induced lung injury in rats, Chem. -Biol. Interact. 94 (1995) 157–164.
[48] C.F. Jones, D.W. Grainger, In vitro assessments of nanomaterial toxicity, Adv. Drug Deliv. Rev. 61 (2009) 438–456.

Biographies

Jing Wang was born in Zhejiang Province, China, in 1986. He received his BS and Ph.D. degree in 2008 and 2013, respectively in Huazhong Agricultural University under the direction of Professor Heyou Han. Presently he is working as a lecturer at Zhejiang University of Technology. His scientific interests focus on functionalized quantum dots for fluorescent and electrochemiluminescent applications.

Na Li was born in Hubei Province, China, in 1986. She received her BS degree in 2010 and now she is a Ph.D. student in Huazhong Agricultural University under the direction of Professor Heyou Han. Her scientific interests focus on functionalized quantum dots for fluorescent sensing and imaging applications.

Feng Shao was in Shandong Province, China, in 1989. He received his MS degree in 2014 in Huazhong Agricultural University under the direction of Professor Heyou Han. His research interests focus on synthesis and modification of plasmonic nanostructures for biosensing and bioimaging.

Heyou Han was born in Anhui Province, China, in 1962. He received his Ph.D. degree in Wuhan University in 2000 and he was a postdoctor in Jeckson State University (America) from 2000 to 2004. He has been a Professor of Huazhong Agricultural University since 2004. He has published over 80 papers in international journals. His research interests focus on functionalized nanomaterials for bioanalytical, food safety and energy applications.